

Library Copy
A. A21 L90

SECURITY INFORMATION

UNCLASSIFIED

Copy 44
RM SL51J22

~~CONFIDENTIAL~~

RA A21 L90

C. -

NACA

RESEARCH MEMORANDUM

for the

Bureau of Aeronautics, Department of the Navy

INVESTIGATION OF THE LOW-SPEED STABILITY AND CONTROL

CHARACTERISTICS OF A $\frac{1}{10}$ - SCALE MODEL OF THE

DOUGLAS XF4D-1 AIRPLANE IN THE

LANGLEY FREE-FLIGHT TUNNEL

TEST NO. NACA DE 349

By Joseph L. Johnson

Langley Aeronautical Laboratory
Langley Field, Va.

CLASSIFICATION CHANGED

UNCLASSIFIED + Unavailable

APR 15 1952
Date

7PA #7

This material contains information affecting the National Defense of the United States within the meaning of the espionage laws, Title 18, U.S.C., Secs. 793 and 794, the transmission or revelation of which in any manner to unauthorized person is prohibited by law.

CLASSIFIED DOCUMENT

NATIONAL ADVISORY COMMITTEE FOR AERONAUTICS

WASHINGTON
UNCLASSIFIED
NOV 1985

~~CONFIDENTIAL~~

NOV 1985



NATIONAL ADVISORY COMMITTEE FOR AERONAUTICS

RESEARCH MEMORANDUM

for the

Bureau of Aeronautics, Department of the Navy

INVESTIGATION OF THE LOW-SPEED STABILITY AND CONTROL

CHARACTERISTICS OF A $\frac{1}{10}$ -SCALE MODEL OF THE

DOUGLAS XF4D-1 AIRPLANE IN THE

LANGLEY FREE-FLIGHT TUNNEL

TED NO. NACA DE 349

By Joseph L. Johnson

SUMMARY

An investigation of the low-speed, power-off stability and control characteristics of a $\frac{1}{10}$ -scale model of the Douglas XF4D-1 airplane has been made in the Langley free-flight tunnel. The model was flown with leading-edge slats retracted and extended over a lift-coefficient range from 0.5 to the stall. Only relatively low-altitude conditions were simulated and no attempt was made to determine the effect on the stability characteristics of freeing the controls.

The longitudinal stability and control characteristics of the model were satisfactory for all conditions investigated except near the stall with slats extended, where the model had a slight nosing-up tendency. The lateral stability and control characteristics of the model were considered satisfactory for all conditions investigated except near the stall with slats retracted, where a change in sign of the static-directional-stability parameter $C_{n\beta}$ caused the model to be directionally divergent. The addition of an extension to the top of the vertical tail did not increase $C_{n\beta}$ enough to eliminate the directional divergence of the model, but a large increase in $C_{n\beta}$ that was obtainable by artificial means appeared to eliminate the divergence and flights near

the stall could be made. Artificially increasing the stability derivatives $-C_{n_r}$ (yawing moment due to yawing) and C_{n_p} (yawing moment due to rolling) had little effect on the divergence for the range of these parameters investigated.

Calculations indicate that the damping of the lateral oscillation of the airplane with slats retracted or extended will be satisfactory at sea level but will be only marginally satisfactory at 40,000 feet.

INTRODUCTION

An investigation of the low-speed stability and control characteristics of a $\frac{1}{10}$ -scale model of the Douglas XF4D-1 airplane has been made in the Langley free-flight tunnel at the request of the Bureau of Aeronautics, Navy Department. The XF4D-1 is a jet-propelled, interceptor-type airplane with a modified delta wing.

The investigation consisted of force and flight tests of the model with slats retracted and extended. The flight tests included a study of the effect of two artificial stabilizing systems on the lateral stability in the high-lift-coefficient range for the model with slats retracted.

In order to permit a better interpretation of the free-flight-tunnel tests in terms of the full-scale airplane, a comparison was made between the results of force tests at low Reynolds numbers in the free-flight tunnel and force tests at higher Reynolds numbers conducted at the Guggenheim Aeronautical Laboratory, California Institute of Technology (GALCIT). Calculations to determine the period and time required to damp to one-half amplitude of the lateral oscillation were also made for the model and full-scale airplane for sea-level and altitude conditions.

SYMBOLS

All stability parameters and coefficients are referred to the stability system of axes originating at a center-of-gravity position of 23.6 percent of the mean aerodynamic chord and vertically on the center line of the model (see fig. 1). The relation of the stability axes to the other axes considered herein is shown in figure 2.

S wing area, square feet

\bar{c}	mean aerodynamic chord, feet
V	airspeed, feet per second
b	wing span, feet
q	dynamic pressure, pounds per square foot
ρ	air density, slugs per cubic foot
W	weight, pounds
m	airplane mass, slugs
μ_b	relative density factor ($m/\rho S b$)
β	angle of sideslip, degrees ($\beta = -\psi$ in force tests)
ψ	angle of yaw, degrees
ϕ	angle of bank, degrees
α	angle of attack of reference axis (fig. 2), degrees
η	angle of attack of principal longitudinal axis of airplane, positive when principal axis is above flight path at nose (fig. 2), degrees
ϵ	angle between reference axis and principal axis, positive when reference axis is above principal axis at nose (fig. 2), degrees
θ	angle between reference axis and horizontal axis, positive when reference axis is above horizontal axis at nose (fig. 2), degrees
γ	angle of flight path to horizontal axis, positive in a climb (fig. 2), degrees
I_X	moment of inertia about reference longitudinal axis, slug-feet ² (mk_X^2)
I_Y	moment of inertia about reference lateral axis, slug-feet ² (mk_Y^2)

I_Z	moment of inertia about reference vertical axis, slug-feet ² (mk_Z^2)
k_{X_0}	radius of gyration about principal longitudinal axis, feet
k_{Z_0}	radius of gyration about principal vertical axis, feet
k_X	radius of gyration about reference longitudinal axis, feet
k_Y	radius of gyration about reference lateral axis, feet
k_Z	radius of gyration about reference vertical axis, feet
K_{X_0}	nondimensional radius of gyration about principal vertical axis (k_{X_0}/b)
K_{Z_0}	nondimensional radius of gyration about principal vertical axis (k_{Z_0}/b)
K_X	nondimensional radius of gyration about longitudinal stability axis $\left(\sqrt{K_{X_0}^2 \cos^2 \eta + K_{Z_0}^2 \sin^2 \eta} \right)$
K_Z	nondimensional radius of gyration about vertical stability axis $\left(\sqrt{K_{Z_0}^2 \cos^2 \eta + K_{X_0}^2 \sin^2 \eta} \right)$
K_{XZ}	nondimensional product-of-inertia parameter $\left((K_{Z_0}^2 - K_{X_0}^2) \cos \eta \sin \eta \right)$
C_L	lift coefficient (Lift/qS)
C_D	drag coefficient (Drag/qS)
C_m	pitching-moment coefficient (Pitching moment/qS \bar{c})
C_n	yawing-moment coefficient (Yawing moment/qSb)
C_l	rolling-moment coefficient (Rolling moment/qSb)

C_Y lateral-force coefficient (Lateral force/ qS)

$$C_{Y\beta} = \frac{\partial C_Y}{\partial \beta} \text{ per degree (per radian in table II)}$$

$$C_{n\beta} = \frac{\partial C_n}{\partial \beta} \text{ per degree (per radian in table II)}$$

$$C_{l\beta} = \frac{\partial C_l}{\partial \beta} \text{ per degree (per radian in table II)}$$

$$C_{Yp} = \frac{\partial C_Y}{\partial \frac{pb}{2V}} \text{ per radian}$$

$$C_{lp} = \frac{\partial C_l}{\partial \frac{pb}{2V}} \text{ per radian}$$

$$C_{np} = \frac{\partial C_n}{\partial \frac{pb}{2V}} \text{ per radian}$$

$$C_{lr} = \frac{\partial C_l}{\partial \frac{rb}{2V}} \text{ per radian}$$

$$C_{Yr} = \frac{\partial C_Y}{\partial \frac{rb}{2V}} \text{ per radian}$$

$$C_{nr} = \frac{\partial C_n}{\partial \frac{rb}{2V}} \text{ per radian}$$

$$C_{n\delta_a} = \frac{\partial C_n}{\partial \delta_a} \text{ per degree}$$

$$C_{l\delta_a} = \frac{\partial C_l}{\partial \delta_a} \text{ per degree}$$

δ_e elevator deflection perpendicular to hinge line (elevons deflected together for elevator control), degrees

δ_a	aileron deflection perpendicular to hinge line (elevons deflected differentially for aileron control), degrees
$\delta_{trimmer}$	trimmer deflection perpendicular to hinge line, degrees
p	rolling angular velocity, radians per second
r	yawing angular velocity, radians per second
$T_{1/2}$	time for amplitude of oscillation to change by factor of 2 (positive value indicates a decrease to half-amplitude; negative value indicates an increase to double amplitude), seconds

APPARATUS AND MODEL

The investigation was conducted in the Langley free-flight tunnel, which is designed to test free-flying dynamic models. A complete description of the tunnel and its operation is presented in reference 1. The rolling derivatives were measured on the rotary balance in the Langley 20-foot free-spinning tunnel which is described in reference 2.

The $\frac{1}{10}$ -scale model used in the investigation was constructed at the Langley Laboratory. A three-view drawing of the model is presented in figure 3 and a photograph of the model is shown in figure 4. Table I gives the mass and dimensional characteristics of the full-scale design and the scaled-up mass and dimensional characteristics of the model. For some tests an extension was added to the top of the design vertical tail for the model in the clean configuration (see fig. 3).

Two artificial stabilizing systems were used on the model in the clean configuration to study their effect on the lateral stability characteristics. One system employed a free-floating vane as a sensing device. The free-floating vane operated an air servomechanism to deflect the rudder in proportion to sideslip angle. The other system used a rate gyro instead of the free-floating vane as the sensing device and actuated an air servomechanism to deflect the rudder in proportion to either yawing or rolling velocities.

DETERMINATION OF THE STATIC STABILITY AND CONTROL

CHARACTERISTICS OF THE FLIGHT TEST MODEL

Force Tests

Force tests were made to determine the static longitudinal and lateral stability and control characteristics of the model over an angle-of-attack range from 0° through the stall for configurations with slats retracted and with slats extended. The static-lateral-stability derivatives were determined for the tail-off and tail-on configurations from measurements of force and moment coefficients at 5° and -5° yaw. All the force tests were run at a dynamic pressure of 3.0 pounds per square foot, which corresponds to an airspeed of about 34.0 miles per hour at standard sea-level conditions and to a test Reynolds number of 582,000 based on the mean aerodynamic chord of 1.825 feet.

The static longitudinal and lateral stability and control characteristics of the model are presented in figures 5 to 10. Also presented for comparison with the free-flight-tunnel data are higher-scale data (Reynolds number 3,510,000) obtained from tests conducted at GALCIT (references 3 and 4). All the GALCIT lateral-stability data are presented for a center-of-gravity position of 25 percent of the mean aerodynamic chord, but the longitudinal data were transferred to a center-of-gravity position of 23.6 percent of the mean aerodynamic chord to permit a direct comparison with the free-flight-tunnel data.

Longitudinal stability and control.- The longitudinal stability and control characteristics of the free-flight-tunnel and GALCIT models with slats retracted and extended are presented in figures 5 to 7. The lift-curve slopes, the maximum lift coefficients, and the drag coefficients for the free-flight-tunnel model were generally lower than those for the GALCIT model, with slats either retracted or extended, because of the lower scale of the free-flight-tunnel tests. A comparison of the pitching-moment curves for the two models shows fair agreement at low and moderate lift coefficients in that both models had about the same static longitudinal stability $-dC_m/dC_L$. The effect of the slat was to decrease the static longitudinal stability of both models. With slats extended the free-flight-tunnel model had a decrease in longitudinal stability at the stall. A comparison of the two sets of data at the stall could not be made since the GALCIT data were not obtained at high enough angles of attack. The trend of the results in the higher-lift-coefficient range for the GALCIT model with slats retracted (fig. 6), however, appeared to be somewhat similar to that of the free-flight-tunnel model; that is, the longitudinal stability increased at the stall.

Elevator and trimmer effectiveness for the two models was not directly comparable since the elevons and trimmers were not deflected to the same angles on both models. For the slats-retracted configuration, the combination of 15° deflection of the elevons as elevators and 30° deflection of the trimmer on the free-flight-tunnel model gave about the same change in pitching moment as 20° deflection of the elevons on the GALCIT model. For approximately the same trimmer and elevon deflections as used on the GALCIT model with slats extended, the free-flight-tunnel model had slightly less change in pitching moment than the GALCIT model (fig. 7).

Lateral stability and control.- The variation of the lateral stability parameters $C_{Y\beta}$, $C_{N\beta}$, and $C_{l\beta}$ with lift coefficient and angle of attack for the free-flight-tunnel and GALCIT models with slats retracted and extended are presented in figures 8 and 9. It should be pointed out that the controls were not deflected to the same angles for the two models. The trimmers on the GALCIT model were held neutral while the elevons were deflected, but on the free-flight-tunnel model the trimmers and elevons were deflected together to provide trim at the high lift coefficients so that the elevons did not have to be deflected to extremely large angles. For the GALCIT model the elevons were changed with angle of attack to correspond to trim conditions at various lift coefficients, but for the free-flight-tunnel model the controls were fixed over the angle-of-attack range for several different control settings. The control settings used on the free-flight-tunnel model represented those required for trim near zero lift and near the stall, so that an approximation of the trimmed lateral-stability parameters can be made over other portions of the angle-of-attack range. It should therefore be kept in mind that any difference in the two sets of data might be partly attributed to the fact that the trimmers on the free-flight-tunnel model were deflected but those on the GALCIT model were held neutral.

The variation of the directional-stability parameter $C_{N\beta}$ and the effective-dihedral parameter $-C_{l\beta}$ with angle of attack and with lift coefficient for the free-flight-tunnel model with slats retracted was generally similar to that for the GALCIT model (fig. 8) except that the break in these stability parameters occurred at a lower lift coefficient for the free-flight-tunnel model than for the GALCIT model. The directional stability of the free-flight-tunnel model was approximately constant up to moderate lift coefficients and then dropped rapidly to negative values at the stall. The GALCIT model had higher directional stability over the lift-coefficient range but, like the free-flight-tunnel model, showed a rapid decrease in $C_{N\beta}$ at the higher lift coefficients. The positive effective dihedral of the two models increased up to moderate lift coefficients and then decreased in the higher lift-coefficient range. As the stall was approached the effective dihedral

changed from positive to negative values for the free-flight-tunnel model and apparently would have also become negative for the GALCIT model if the data had been obtained to high enough angles of attack.

The results presented in figure 8 show that the addition of an extension to the top of the design vertical tail to increase the area by 8 percent increased the vertical tail contribution to $C_{n\beta}$ by about 35 percent at zero angle of attack. In the higher angle-of-attack range the $C_{n\beta}$ produced by the extension decreased and the angle of attack at which $C_{n\beta}$ of the model became zero was extended only slightly.

With the slats extended (fig. 9) the linear range of $C_{n\beta}$ and $-C_{l\beta}$ was extended to higher lift coefficients for both the free-flight-tunnel model and the GALCIT model. The directional stability of the free-flight-tunnel model still decreased to zero as the stall was approached but the decrease was not as rapid, and the instability at the higher angles of attack was much less than the instability of the slats-retracted configuration. The effective dihedral for this model increased up to moderate lift coefficients and remained at a fairly large positive value through the stall. The GALCIT model generally had greater directional stability and effective dihedral than the free-flight-tunnel model over the angle-of-attack range for which the GALCIT data were obtained.

The results of tests made to determine the aileron effectiveness of the free-flight-tunnel and GALCIT models are presented in figure 10. These results show that the rolling moment produced by a given aileron deflection for both models is greater for the slats-retracted configuration than for the slats-extended configuration. This difference can be attributed to the difference in the trim elevon settings used for the two configurations (-15° for the slats-retracted configuration and -23° for the slats-extended configuration). Deflecting the elevons as ailerons 15° from the trim position resulted in a deflection of 38° for the slats-extended configuration, which was in the range where the aileron effectiveness decreased rapidly. The GALCIT model had greater effectiveness than the free-flight-tunnel model for a given configuration, probably because of the higher Reynolds number of the GALCIT tests. A comparison of the results of figure 10 shows that the yawing moment due to aileron deflection was generally about the same for both models over the lift-coefficient range.

Rotary Tests

Rotary tests were made to determine the rolling derivatives for the model with controls neutral and deflected, with the slats retracted and

extended, and with the design vertical tail off and on. All rotary tests were run at a dynamic pressure of 5.5 pounds per square foot, which corresponds to an airspeed of approximately 46.5 miles per hour at standard sea-level conditions and to an effective Reynolds number of 793,000 based on the mean aerodynamic chord of 1.825 feet.

Rotary-test data for the model with controls neutral (fig. 11(a)) and with controls deflected (fig. 11(b)) show a rapid decrease in the damping-in-roll parameter $-C_{l_p}$ at the higher angles of attack with slats retracted or extended. Extending the slats delayed the decrease in $-C_{l_p}$ to a higher angle of attack but resulted in a greater decrease when it occurred. The vertical tail contributed very little damping in roll over the angle-of-attack range, but deflecting the controls increased substantially the damping in roll. The yawing moment due to rolling C_{n_p} for the complete model with slats retracted or extended reached large negative values in the higher angle-of-attack range because of the large negative increment contributed by the vertical tail. The effect of extending the slats was to delay the rapid increase in $-C_{n_p}$ at the higher angles of attack for the tail-on configuration, and the effect of deflecting the controls was to decrease $-C_{n_p}$ in the higher angle-of-attack range. The lateral force due to rolling C_{y_p} was positive over the angle-of-attack range for all configurations tested.

FLIGHT TESTS

Flight tests were made from a lift coefficient of about 0.5 through the stall to determine the dynamic stability and control characteristics of the model with slats retracted and extended. No attempt was made in the flight tests to determine the effect of freeing the controls. All the flight tests with slats retracted were made at a center-of-gravity position of 23.6 percent of the mean aerodynamic chord. The flight tests with slats extended were made over a center-of-gravity range from 20.2 percent to 23.6 percent of the mean aerodynamic chord.

Most of the flights were made at the light loading (table I) in order to minimize damage to the model in crack-ups, but a few flights were made with the model at a heavier loading so that it had approximately the correct scaled-down values of the radii of gyration of the full-scale airplane and simulated the mass density of the airplane at about 10,000 feet.

Included in the flight tests was a study of the effect of large variations in the derivatives C_{n_r} , C_{n_p} , and C_{n_β} on the lateral

stability and control characteristics of the model in the clean configuration. These derivatives were varied by the use of the artificial stabilizing devices described in a preceding section.

CALCULATIONS

Calculations were made by the method of reference 5 to determine the period and time to damp to one-half amplitude of the lateral oscillatory mode and the time to damp to one-half amplitude of the aperiodic modes for the model with slats retracted and extended in the light condition and also for the full-scale airplane with slats retracted and extended at the normal gross weight.

The aerodynamic and mass characteristics used in the calculations are presented in table II. Values of C_{Y_β} , C_{n_β} , and C_{l_β} for the model were obtained from force tests made in the free-flight tunnel and those for the airplane were obtained from reference 4. The tail-off values of C_{Y_r} , C_{n_r} , and C_{l_r} were estimated from references 6 and 7 for both the model and the airplane. The contribution of the vertical tail to the stability derivatives C_{Y_r} , C_{n_r} , and C_{l_r} for both the model and the airplane was estimated from the equations given at the bottom of table II, which are similar to those given in reference 8. Values of C_{Y_p} , C_{n_p} , and C_{l_p} were obtained from the data of figure 11 for both the model and the airplane. The rotary derivatives for the airplane were obtained by extrapolating the data of figure 11 to the higher-scale lift characteristics obtained from reference 3.

FLIGHT TEST RESULTS AND DISCUSSION

Interpretation of Flight Test Results

In interpreting the results of the model flight tests in terms of the full-scale airplane it is necessary to consider any differences between the aerodynamic and scaled-up mass characteristics of the model and those of the full-scale airplane. If the airplane has the same mass and static stability characteristics and the same rotary derivatives as those of the model, the airplane would be expected to exhibit dynamic characteristics similar to those of the free-flight-tunnel model.

It has been shown that the static stability characteristics of the low-scale, free-flight-tunnel model are in fair agreement with the higher-scale results of the GALCIT model except that the free-flight-tunnel model

stalls at a lower lift coefficient and consequently the stability derivatives for the free-flight-tunnel model depart from linearity at lower lift coefficients than those for the GALCIT model. The dynamic behavior of the airplane is therefore expected to be similar to that of the free-flight-tunnel model except that corresponding dynamic behavior should occur at higher lift coefficients for the airplane than for the model.

As pointed out in a preceding section, flight tests were made with the model in both a lightly loaded and a heavily loaded condition. The lightly loaded model had values of the scaled-up radii of gyration and moments of inertia somewhat higher than those for the airplane at normal gross weight, but the wing loading was lower for the model than for the airplane (see table I). In order to simulate more nearly the radii of gyration of the airplane, the model was loaded by placing weight at approximately its center of gravity. In this heavier condition the radii of gyration of the model were reduced so that they approximately corresponded to those of the airplane. The added weight increased the wing loading of the model beyond that of the airplane so that the mass density of the model simulated that of the airplane flying at an altitude of about 10,000 feet. Flight tests indicated that for the range of mass parameters investigated the longitudinal and lateral stability and control and the general flight behavior for the heavy condition were about the same as those for the light condition. No distinction will therefore be made between the light and heavy loadings in the discussion of results.

It should be pointed out that the full-scale airplane should be easier to fly than the model because its angular velocities are about one-third as fast as those of the model. Another factor which should make it easier for the pilot to control the airplane is the fact that he has independent aileron and rudder control rather than coordinated aileron and rudder control such as that used on the model.

Longitudinal Stability and Control

The longitudinal stability and control characteristics of the model were considered satisfactory for all conditions investigated except near the stall with slats extended. As the stall was approached, the model with slats extended became longitudinally unstable but the nosing-up tendency resulting from this instability could be controlled by the elevator. When the center of gravity was moved from 23.6 to 20.2 percent of the mean geometric chord, the nosing-up tendency was reduced but was still considered to be objectionable. If no effort was made to control the nosing-up tendency the model would stall and settle gently to the tunnel floor with some elevon effectiveness being retained.

Flights near the stall with slats retracted could not be made because of lateral-stability difficulties that caused the model to crash

before the longitudinal stability and control characteristics could be determined. It is believed, however, that the dynamic longitudinal stability and control characteristics for this configuration will be satisfactory through the stall, since the results of static tests indicate satisfactory characteristics in the higher lift range.

Although the longitudinal stability characteristics of the model were considered to be generally satisfactory, some difficulty was encountered in flying the model in the high-lift-coefficient range because of the large variation of drag with lift, which is generally a characteristic of swept wings with low aspect ratio (see reference 9). This large variation of drag with lift caused large variations of glide angle with lift coefficient, since the trim glide angle is a function of the drag-lift ratio. The minimum glide angle occurred at a fairly low lift coefficient for the model instead of near the stall as with conventional models. When the model was trimmed to fly at a lift coefficient below that corresponding to the minimum glide angle, the response of the model to elevator control was normal; that is, deflecting the elevator downward increased the glide angle and deflecting the elevator upward decreased the glide angle. When the model was trimmed to fly at a lift coefficient above that corresponding to the minimum glide angle, however, a deflection of the elevator downward caused the glide angle to become steeper for a short time until the speed of the model increased and approached the new trim speed. The glide angle then became flatter as the model approached the new trim condition. The opposite dynamic behavior followed an upward elevator deflection; that is, the glide angle at first was flatter and then became steeper as the new trim condition was approached.

Flight tests of full-scale, land-based airplanes with low-aspect-ratio wings have demonstrated that elevator control characteristics of this type do not appear to be a very serious problem, and normal landing approaches can apparently be made without the difficulty encountered with low-aspect-ratio models in the free-flight tunnel. It should be pointed out that the technique used in flying models in the free-flight tunnel probably makes this problem appear much worse than it is in the full-scale airplane, since the limited space of the tunnel makes necessary constant corrections of the tunnel angle and airspeed for small changes in trim of the model if sustained flight is to be maintained. Since the XF4D-1 airplane was designed for carrier-based operation, it will require a more precise technique in landing than that for a land-based airplane, and it is possible that even slightly abnormal elevator control characteristics in the high-lift-coefficient condition might be objectionable.

Lateral Stability and Control

Slats retracted.- The lateral stability characteristics of the model with slats retracted were satisfactory over the speed range investigated except near the stall. The lateral oscillations were well-damped over the lift-coefficient range investigated but the model was directionally divergent near the stall. A flight record of the model at a lift coefficient near the stall ($C_L = 0.70$) with slats retracted (fig. 12(a)) shows that the model yawed to an angle of about 50° and rolled to an angle of about 90° before crashing into the side of the tunnel wall. This behavior was characteristic of each attempted flight at this and higher lift coefficients, despite efforts by the pilot to keep the model flying. The rapid divergence in yaw was attributed to the fact that the model became statically directionally unstable in the higher angle-of-attack range (see fig. 8). Flights were very short because the model usually yawed on take-off, which made sustained flights impossible. The recording cameras were usually turned on just prior to take-off of the model so that records of the brief flights could be obtained.

Calculated values of the damping of the lateral modes of motion for the slats-retracted condition are in qualitative agreement with the flight tests in that they show good damping of the oscillatory mode and instability of one of the aperiodic modes at high lift coefficients (see table II).

The addition of an extension to the top of the design vertical tail to increase $C_{n\beta}$ had no apparent effect on the directional divergence, and the small delay in lift coefficient at which the directional stability became negative was not apparent in flight tests of the model.

The use of the free-floating-vane system to increase artificially the static-directional-stability parameter $C_{n\beta}$ in an effort to overcome the directional divergence improved the flight behavior of the model to such an extent that flights near the stall could be made (see fig. 12(b)). Although the yawing motions were still present, the system showed definite promise of completely eliminating the directional divergence near the stall.

In order to study the effect of varying other derivatives as a means of eliminating the directional divergence of the model, the derivative $-C_{nr}$ was artificially increased by the use of a rate gyro to add damping to the yawing motion. Flight tests indicated that artificially increasing $-C_{nr}$ alone did not eliminate the directional divergence of the model but the yawing motion was slower than in the case of the basic model (fig. 12(c)). In any event, the amount of C_{nr} used in these flight tests (-1.05) was not sufficient to give satisfactory flight characteristics

and did not appear to be as effective in improving the lateral stability characteristics as artificially increasing $C_{n\beta}$.

In a further study of the effect of varying other derivatives as a means of eliminating the directional divergence of the model, the derivatives C_{np} and $-C_{nr}$ were artificially increased simultaneously. The derivative C_{np} was increased to eliminate the adverse yawing moment due to rolling (fig. 11) and the derivative $-C_{nr}$ was increased to add damping to the yawing motion. Small changes in the value of C_{np} had no effect on the flight characteristics and it was therefore necessary to increase this derivative to large values before its effect could be determined. With $-C_{nr}$ artificially increased to a value of -0.45 and C_{np} artificially increased to a value of 0.83 , the flight behavior of the model was found to be a little worse than that for the basic condition as shown by the flight record of figure 12(d). Although increasing C_{np} and $-C_{nr}$ probably increased the oscillatory stability, and the greater $-C_{nr}$ slowed down the yawing motion, the increased yawing moment due to rolling apparently tended to reinforce the directional divergence so that the model rolled and yawed even more violently than in the basic condition.

The lateral control characteristics were considered satisfactory over the low- and medium-lift-coefficient range. In the high-lift-coefficient range the model yawed around and crashed before any evaluation of the control characteristics could be made.

Slats extended.- The lateral stability characteristics of the model with slats extended were satisfactory over the speed range and there was no evidence of a directional divergence despite the fact that the static-directional-stability parameter $C_{n\beta}$ decreased to zero and became negative in the higher-angle-of-attack range (fig. 9). The difference in the behavior of the model near the stall with slats retracted and with slats extended was attributed to the differences in $C_{n\beta}$ and effective dihedral $-Cl_{\beta}$. As pointed out in a previous section, $C_{n\beta}$ did become negative as the stall was approached with slats extended but did not become nearly as strongly negative as with slats retracted (figs. 8 and 9). The effective dihedral remained high through the stall with slats extended, whereas with slats retracted (fig. 8) the effective dihedral decreased to zero. Stability theory shows that an airplane can be directionally stable with three degrees of lateral freedom even though $C_{n\beta}$ is negative, provided the dihedral effect is positive (reference 10).

The calculated damping characteristics indicated that the model with slats extended should have become oscillatorily unstable at the higher lift coefficients while the aperiodic mode remained stable (table II). Brief calculations made to study the effect of the various parameters on the lateral oscillation for the model indicated that the decrease in damping in roll at high lift coefficients was the principal reason that the calculated lateral oscillation became unstable. The cause of this discrepancy between the flight tests and calculations is not known but it appears that in the flight tests at a given angle of attack the model must have had a higher value of C_{lp} than indicated by the rotary-test data of figure 11.

The lateral control characteristics were considered satisfactory over the lift range investigated, including the stall. At the higher lift coefficients there was some evidence of adverse yawing with ailerons alone because of the adverse yawing due to aileron deflection (fig. 10) and also the adverse yawing due to roll (fig. 11). This adverse yawing was not very objectionable, however, and could be eliminated entirely by using the rudder in combination with the aileron for coordinated control. When the model stalled there was no sign of abrupt rolling or yawing and the model settled gently to the tunnel floor. The ailerons and rudder were effective for controlling the model through the stall. It should be pointed out that full-scale flight tests of tailless airplanes having sweptback wings of low aspect ratio have indicated more severe adverse yawing characteristics than were demonstrated by models of these airplanes flown in the free-flight tunnel. This difference in yawing characteristics is attributed to the fact that the derivative $-C_{np}$ remains linear over a greater range of lift coefficients for the airplane, resulting in greater adverse yawing due to rolling at high angles of attack for the airplane than for the model. Also, the airplane requires less up deflection of the control surfaces for trim at the higher lift coefficients, which would probably result in the airplane having more adverse yawing due to aileron deflection than the model. On this basis, therefore, it is expected that any adverse yawing behavior of the full-scale airplane will probably be more severe than that indicated from flight tests of the model.

Calculated lateral stability characteristics for full-scale airplane.-
The results of calculations made to determine the period and damping of the full-scale airplane at lift coefficients of 0.55 and 0.80 for sea level and 40,000 feet are presented in table II. These results are plotted in figure 13, together with the U. S. Navy flying-qualities requirements for satisfactory damping of the lateral oscillation (reference 11). Also plotted in figure 13 are the calculated damping results obtained from reference 4 for the airplane at a lift coefficient of 0.55 at sea level and 40,000 feet. These results indicate that the damping of the airplane with slats retracted or extended should be satisfactory at sea level but should be only marginally satisfactory at 40,000 feet.

The slight difference between the calculated results of the free-flight tunnel and reference 4 can be attributed to differences in the derivatives used, as shown in table II. The results of calculations from reference 4 indicate that the airplane should be less satisfactory at lower lift coefficients at both sea level and 40,000 feet.

SUMMARY OF RESULTS

The following conclusions were drawn from the results of the free-flight-tunnel stability and control investigation on a $\frac{1}{10}$ -scale model of the Douglas XF4D-1 airplane. The model was flown with leading-edge slats retracted and extended over a lift-coefficient range from 0.5 to the stall. Only low-speed and relatively low-altitude conditions were simulated and no attempt was made to determine the effect on the stability characteristics of freeing the controls.

1. The longitudinal stability and control characteristics of the model were considered satisfactory for all conditions investigated except near the stall with slats extended, where the model had a slight nosing-up tendency.
2. The lateral stability and control characteristics of the model were considered satisfactory for all conditions investigated except near the stall with slats retracted, where a change in sign of the static-directional-stability parameter $C_{n\beta}$ caused the model to be directionally divergent. With slats extended the lateral stability and control was considered to be satisfactory over the speed range, including the stall.
3. The addition of an extension to the top of the vertical tail did not increase $C_{n\beta}$ enough to eliminate the directional divergence of the model, but the large increase in $C_{n\beta}$ that was obtainable by artificial means appeared to eliminate the divergence with the result that flights near the stall could be made. Artificially increasing the stability derivatives $-C_{nr}$ (yawing moment due to yawing) and C_{np} (yawing moment due to rolling) had little effect on the divergence for the range of these parameters investigated.

4. Calculations indicate that the damping of the lateral oscillation of the airplane with slats retracted or extended will be satisfactory at sea level but will be only marginally satisfactory at 40,000 feet.

Langley Aeronautical Laboratory
National Advisory Committee for Aeronautics
Langley Field, Va.



Joseph L. Johnson
Aeronautical Research Scientist

Approved: *Thomas A. Harris*
Thomas A. Harris
Chief of Stability Research Division

mjw

REFERENCES

1. Shortal, Joseph A., and Osterhout, Clayton J.: Preliminary Stability and Control Tests in the NACA Free-Flight Wind Tunnel and Correlation with Full-Scale Flight Tests. NACA TN 810, 1941.
2. Stone, Ralph W., Jr., Burk, Sanger M., Jr., and Bihrlle, William, Jr.: The Aerodynamic Forces and Moments on a $\frac{1}{10}$ -Scale Model of a Fighter Airplane in Spinning Attitudes as Measured on a Rotary Balance in the Langley 20-Foot Free-Spinning Tunnel. NACA TN 2181, 1950.
3. Pounder, Edwin: Report on Wind-Tunnel Tests of a 0.1791 Scale Model of the Douglas (El Segundo) XF⁴D-1 Airplane. GALCIT Rep. No. 555, Nov. 23, 1949.
4. Huff, W. W., Jr.: Stability and Control Characteristics of Douglas Model XF⁴D-1. Part I. Low Speed Flying Qualities. Rep. No. ES 1530⁴, Douglas Aircraft Co., Inc., Nov. 8, 1949.
5. Sternfield, Leonard: Some Considerations of the Lateral Stability of High-Speed Aircraft. NACA TN 1282, 1947.
6. Letko, William, and Cowan, John W.: Effect of Taper Ratio on Low-Speed Static and Yawing Stability Derivatives of 45° Sweptback Wings with Aspect Ratio of 2.61. NACA TN 1671, 1948.
7. Campbell, John P., and Goodman, Alex: A Semiempirical Method for Estimating the Rolling Moment Due to Yawing of Airplanes. NACA TN 1984, 1949.
8. Campbell, John P., and McKinney, Marion O.: Summary of Methods for Calculating Dynamic Lateral Stability and Response and for Estimating Lateral Stability Derivatives. NACA TN 2409, 1951.
9. McKinney, Marion O., Jr., and Drake, Hubert M.: Flight Characteristics at Low Speed of Delta-Wing Models. NACA RM L7K07, 1948.
10. Campbell, John P., and Seacord, Charles L., Jr.: The Effect of Mass Distribution on the Lateral Stability and Control Characteristics of an Airplane as Determined by Tests of a Model in the Free-Flight Tunnel. NACA Rep. 769, 1943. (Formerly NACA ARR 3H31.)
11. Anon.: Specification for Flying Qualities of Piloted Airplanes. NAVAER SR-119B, Bur. Aero., June 1, 1948.

TABLE I
 MASS AND DIMENSIONAL CHARACTERISTICS OF THE DOUGLAS XF4D-1 AIRPLANE
 AND SCALED-UP CHARACTERISTICS OF THE $\frac{1}{10}$ -SCALE MODEL
 TESTED IN THE LANGLEY FREE-FLIGHT TUNNEL

	Scaled-up		Full-scale fighter at normal gross weight
	Light	Heavy	
Weight, lb	13,000	22,000	16,821
Wing loading, W/S, lb/sq ft	23.3	39.5	30.2
Relative density factor, μ_R	9.05	15.3	11.77
Moments of inertia: ¹			
I_X , slug-ft ²	14,400	14,400	10,346
I_Z , slug-ft ²	62,600	62,600	40,630
I_Y , slug-ft ²	53,600	53,600	31,492
Radius of gyration to wing span:			
k_X/b	0.178	0.137	0.133
k_Z/b	0.372	0.285	0.263
k_Y/b	0.344	0.264	0.233
Wing:			
Airfoil designation (reference 4)			
Root section			NACA 0007-63/30-9.5° modified
Tip section			NACA 0004.5-63/30-9.5° modified
Area, sq ft			557
Span, ft			33.5
Aspect ratio			2.02
Root chord, ft			25.08
Tip chord, ft			8.33
Taper ratio			0.332
\bar{c} , ft			18.25
Longitudinal distance from leading edge of root chord to leading edge of mean aerodynamic chord, ft			8.95
Sweepback of leading edge, deg			52.5
Dihedral, deg			0
Incidence, deg			0
Slats:			
Span, percent wing span (two)			54.2
Chord, percent wing chord parallel to fuselage reference line			12.68
Elevons:			
Area aft of hinge line, percent wing area (two)			8.1
Span, percent wing span (two)			66.7
Chord parallel to fuselage reference axis, ft			2.16
Trimmer:			
Area aft of hinge line, percent wing area (two)			3.84
Span, percent wing span (two)			20.4
Root chord, ft			4.97
Tip chord, ft			1.675
Vertical tail:			
Airfoil section (reference 4)			
Root section			NACA 0008-63/30-9°
Tip section			NACA 0006-63/30-6°45'
Area, sq ft			47.7
Span, ft			7.58
Aspect ratio			1.20
Taper ratio			0.331
Mean aerodynamic chord, ft			6.86
Rudder:			
Area, sq ft			12.7
Span, ft			6.08
Chord, percent tail chord parallel to fuselage reference axis			30

¹Moments of inertia for the heavy condition were assumed to be the same as for the light condition because the wing loading of the model was increased by adding weight at approximately the center of gravity.



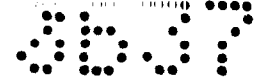


TABLE II
 CHARACTERISTICS OF THE $\frac{1}{10}$ - SCALE MODEL AND FULL-SCALE XF4D-1 AIRPLANE AND RESULTS OF CALCULATIONS
 TO DETERMINE THE PERIOD AND TIME TO DAMP TO ONE-HALF AMPLITUDE

Model

Condition	Slots	a (deg)	C _L	$(\frac{kX_0}{b})^2$	$(\frac{kZ_0}{b})^2$	η (deg)	K _X ²	K _Z ²	K _{XZ}	tan α	μ_b	$\frac{m}{\rho S V}$	C _{1p}	C _{np}	C _{yp}	C _{1r}	C _{nr}	C _{yr}	C _{1\beta}	C _{n\beta}	C _{y\beta}	Oscillatory mode		Aperiodic modes	
																						Period (sec)	T _{1/2} (sec)	Rolling T _{1/2} (sec)	Spiral T _{1/2} (sec)
Light	Retracted	16.5	.55	.0320	.138	13.90	.0381	.1320	.0247	-2.773	9.05	.508	-.187	-.0125	.085	.025	-.0673	.158	-.0602	.0304	-.287	1920	480	.240	3939
		220	.70	.0320	.138	19.40	.0437	.1263	.0332	-3839	9.05	.574	-.120	-.0800	.080	-.038	-.0535	.129	-.0086	-.043	-.309	13594	256	.380	-.95
	Extended	19.5	.55	.0320	.146	16.90	.0410	.1367	.0319	-2586	9.54	.523	-.212	-.0320	.156	.057	-.0600	.153	-.1031	.0275	-.298	1557	2.20	.242	4810
		250	.70	.0320	.146	22.40	.0480	.1294	.0404	-3346	9.54	.590	-.105	-.0300	.125	.050	-.0858	.172	-.1003	.0185	-.235	1578	-5.95	.361	3020

¹The value of a for the model was obtained from flight tests at the given lift coefficient.

Airplane

Source	Altitude	Slots	a (deg)	C _L	$(\frac{kX_0}{b})^2$	$(\frac{kZ_0}{b})^2$	η (deg)	K _X ²	K _Z ²	K _{XZ}	tan α	μ_b	$\frac{m}{\rho S V}$	C _{1p}	C _{np}	C _{yp}	C _{1r}	C _{nr}	C _{yr}	C _{1\beta}	C _{n\beta}	C _{y\beta}	Oscillatory mode		Aperiodic modes	
																							Period (sec)	T _{1/2} (sec)	Rolling T _{1/2} (sec)	Spiral T _{1/2} (sec)
FFT	Sea level	Retracted	140	.55	.0178	.069	13.63	.0206	.0662	.0117	-.1910	11.77	1.835	-.250	0	.090	.051	-.1022	.242	-.0831	.0831	-.401	3.470	2.25	.437	15.500
			210	.80	.0178	.069	20.63	.0241	.0630	.0169	-.2867	11.77	2.213	-.210	-.065	.080	-.042	-.1220	.189	-.0172	.0230	-.401	7.060	6.22	.643	6.300
		Extended	145	.55	.0178	.069	14.13	.0207	.0659	.0121	-.1998	11.77	2.140	-.265	-.035	.200	.085	-.0970	.242	-.1289	.0830	-.401	3.040	2.42	.490	18.550
			215	.80	.0178	.069	21.13	.0244	.0623	.0172	-.2568	11.77	2.580	-.260	-.030	.140	.089	-.1000	.206	-.1524	.1031	-.401	2.923	2.30	.700	15.600
	40,000 ft	Retracted	140	.55	.0178	.069	13.63	.0206	.0662	.0117	-.1910	48.20	3.680	-.250	0	.090	.051	-.1022	.242	-.0831	.0831	-.401	3.260	3.69	.955	31.200
			210	.80	.0178	.069	20.63	.0241	.0626	.0169	-.2867	48.20	4.430	-.210	-.065	.080	-.042	-.1217	.189	-.0172	.0229	-.401	6.880	11.56	1.430	12.700
		Extended	145	.55	.0178	.069	14.13	.0207	.0659	.0121	-.1998	48.20	3.680	-.265	-.035	.200	.085	-.0966	.242	-.1289	.0831	-.401	2.921	3.719	.886	31.800
			215	.80	.0178	.069	21.13	.0244	.0623	.0172	-.2568	48.20	4.430	-.260	-.030	.140	.089	-.1001	.206	-.1524	.1031	-.401	2.809	3.69	1.260	26.800
Douglas (Ref. 4)	Sea level	Retracted	---	.55	.0178	.069	13.50	.0224	.0718	.0136	----	11.77	1.835	-.196	-.016	.300	.135	-.0825	.107	-.1300	.0831	-.338	3.000	2.40	----	----
	40,000 ft		---	.55	.0178	.069	13.50	.0224	.0718	.0136	----	48.20	3.680	-.196	-.016	.300	.135	-.0825	.107	-.1300	.0831	-.338	2.970	4.17	----	----

$$C_{1r \text{ tail}} = 2 \left(\frac{C_{n\beta \text{ tail}}}{C_{y\beta \text{ tail}}} \right) C_{1\beta \text{ tail}}$$

$$C_{nr \text{ tail}} = 2 \left(\frac{C_{n\beta \text{ tail}}}{C_{y\beta \text{ tail}}} \right)^2$$

$$C_{yr \text{ tail}} = 2 C_{n\beta \text{ tail}}$$



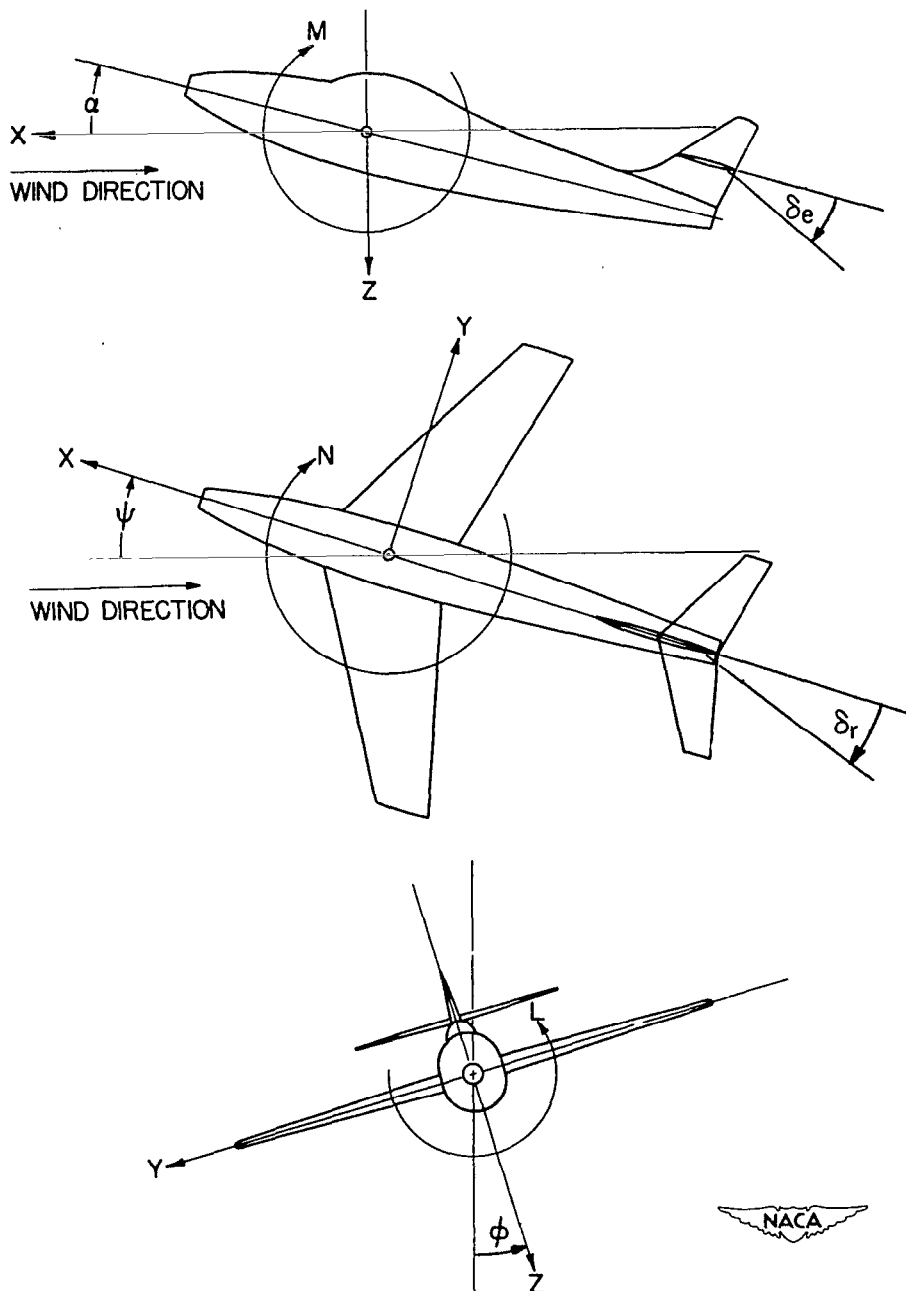


Figure 1.- The stability system of axes. Arrows indicate positive directions of moments, forces, and control-surface deflections. This system of axes is defined as an orthogonal system having the origin at the center of gravity and in which the Z-axis is in the plane of symmetry and perpendicular to the relative wind, the X-axis is in the plane of symmetry and perpendicular to the Z-axis, and the Y-axis is perpendicular to the plane of symmetry.

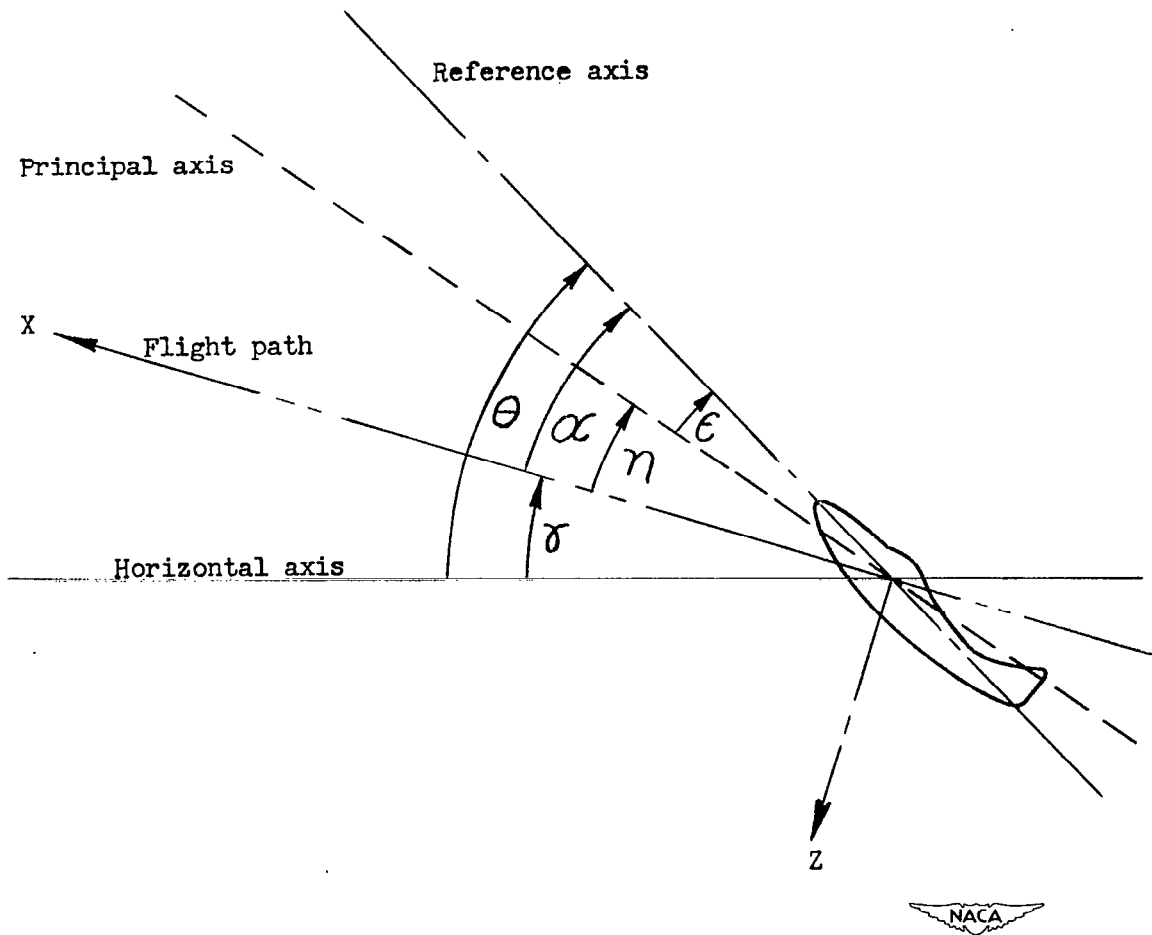


Figure 2.- System of axes and angular relationship in flight. Arrows indicate positive direction of angles. $\eta = \theta - \gamma - \epsilon$.

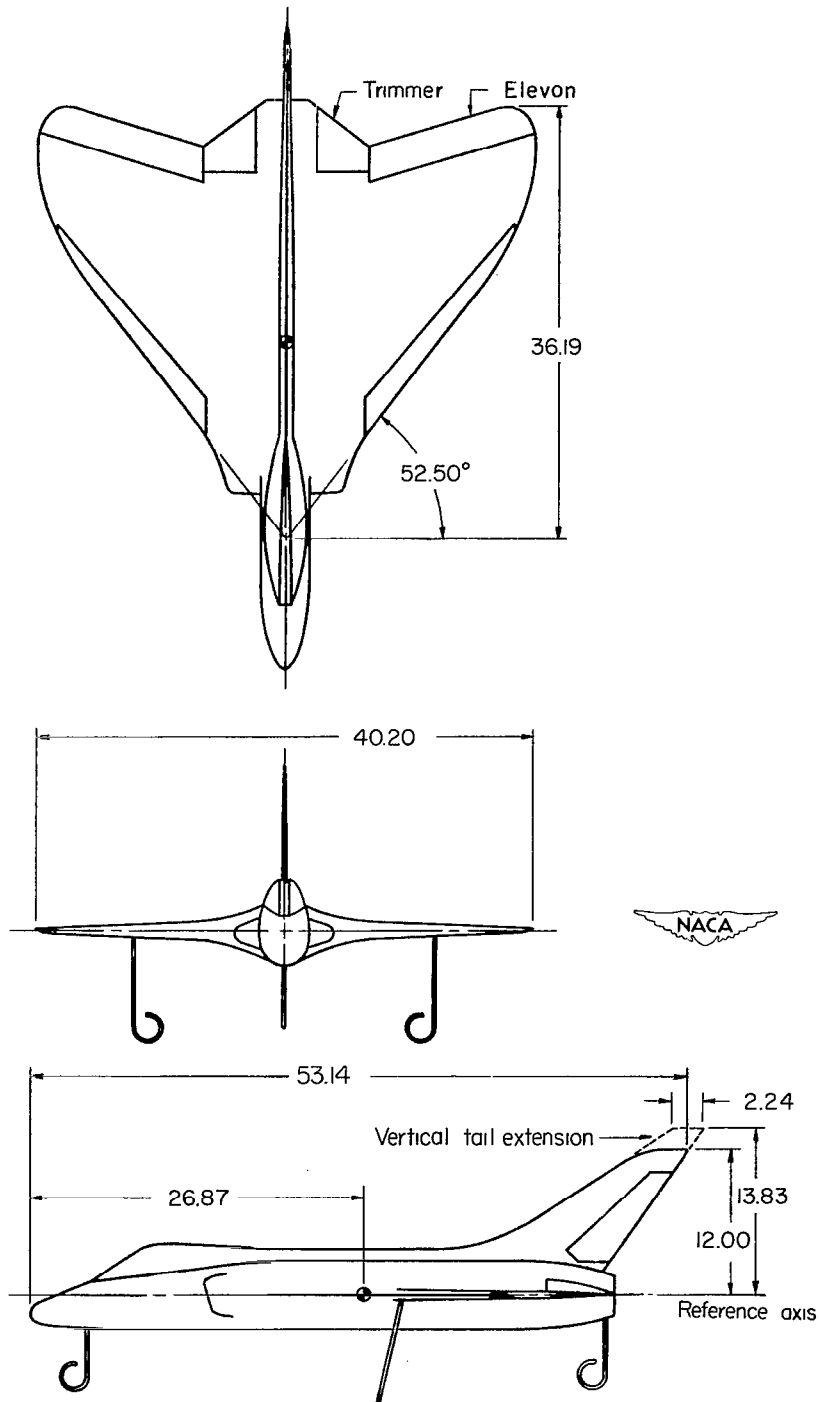


Figure 3.- Three-view drawing of a $\frac{1}{10}$ - scale model of the Douglas XF4D-1 airplane tested in the Langley free-flight tunnel. All dimensions are in inches.

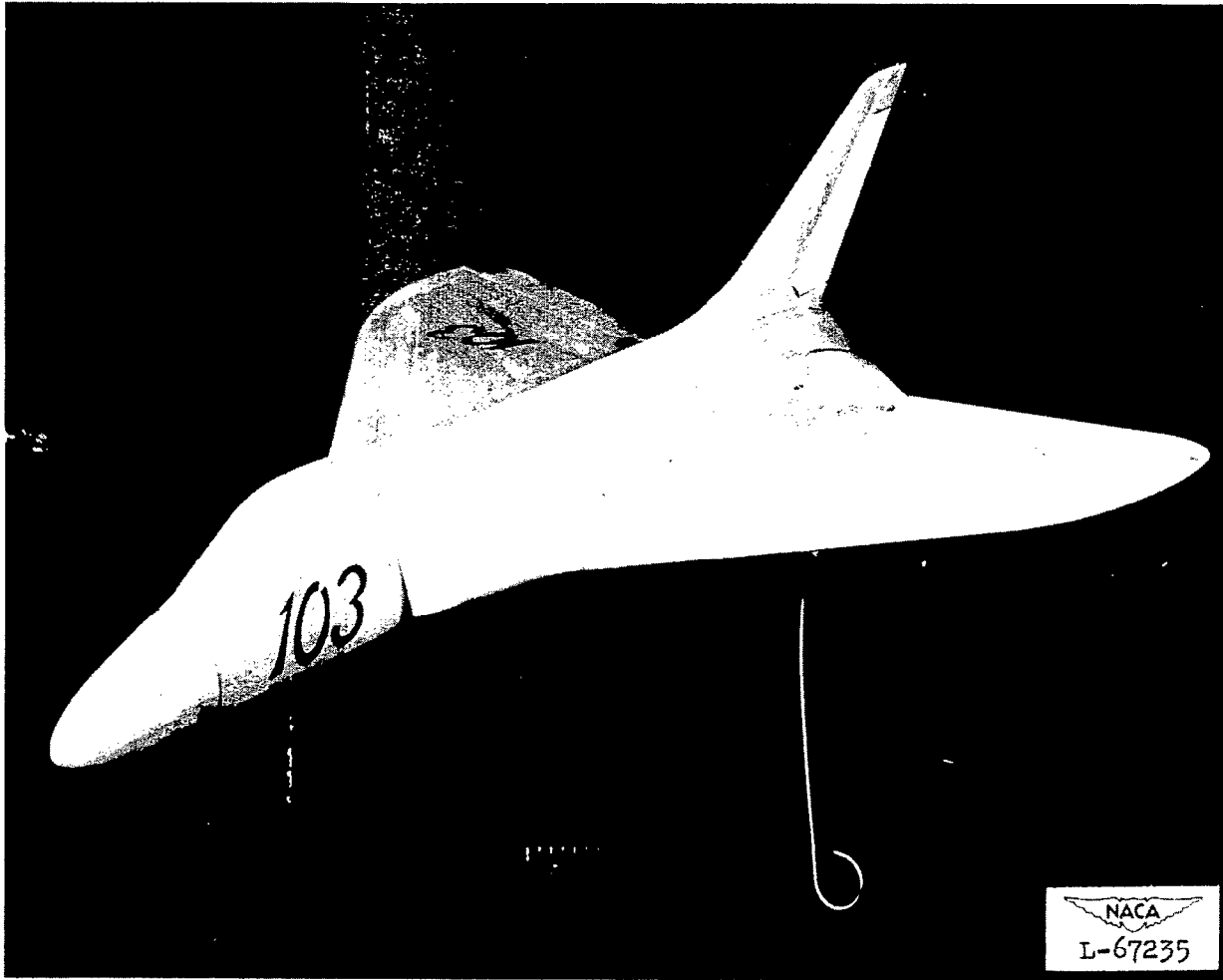


Figure 4.- Photograph of $\frac{1}{10}$ -scale model of the Douglas XF4D-1 airplane tested in the Langley free-flight tunnel.

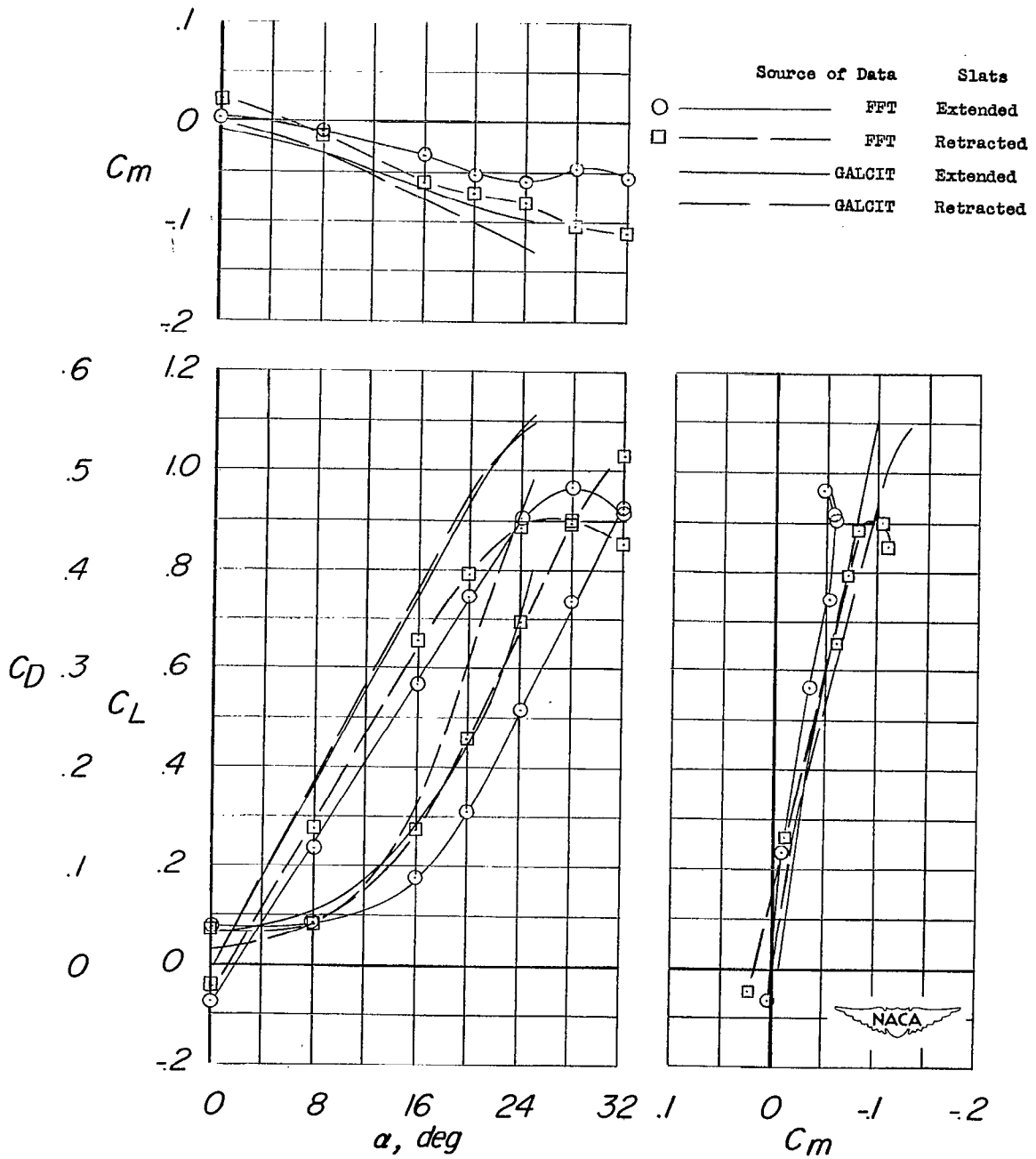


Figure 5.- Comparison of aerodynamic characteristics of a $\frac{1}{10}$ -scale model of the XF4D-1 airplane tested in the Langley free-flight tunnel and a 0.1791-scale model tested at GALCIT. $\delta_e = 0^\circ$; $\delta_{trimmer} = 0^\circ$.

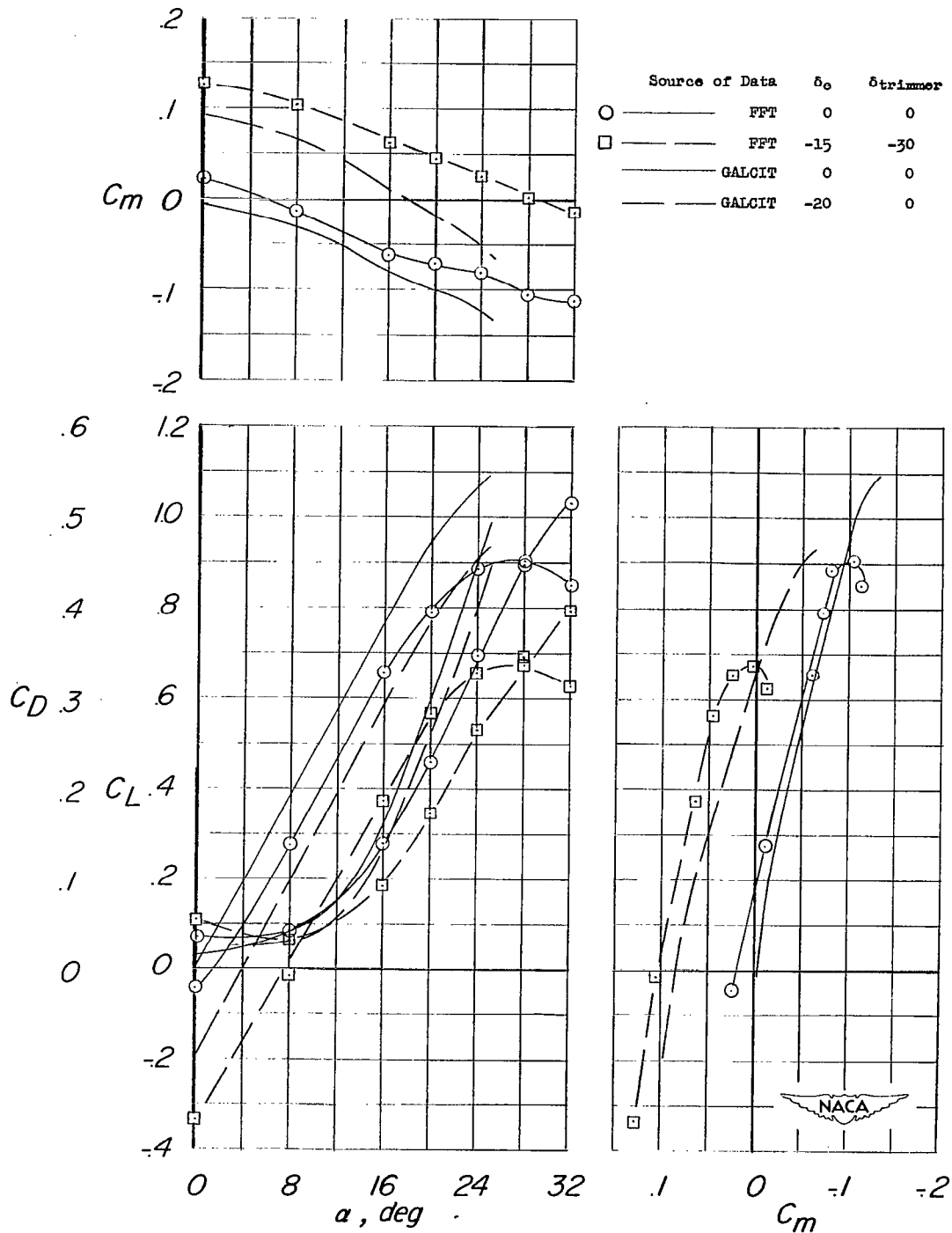


Figure 6.- Effect of elevon and trimmer deflection on the aerodynamic characteristics of a $\frac{1}{10}$ -scale model of the XF4D-1 airplane tested in the Langley free-flight tunnel and a 0.1791-scale model tested at GALCIT. Slats retracted.

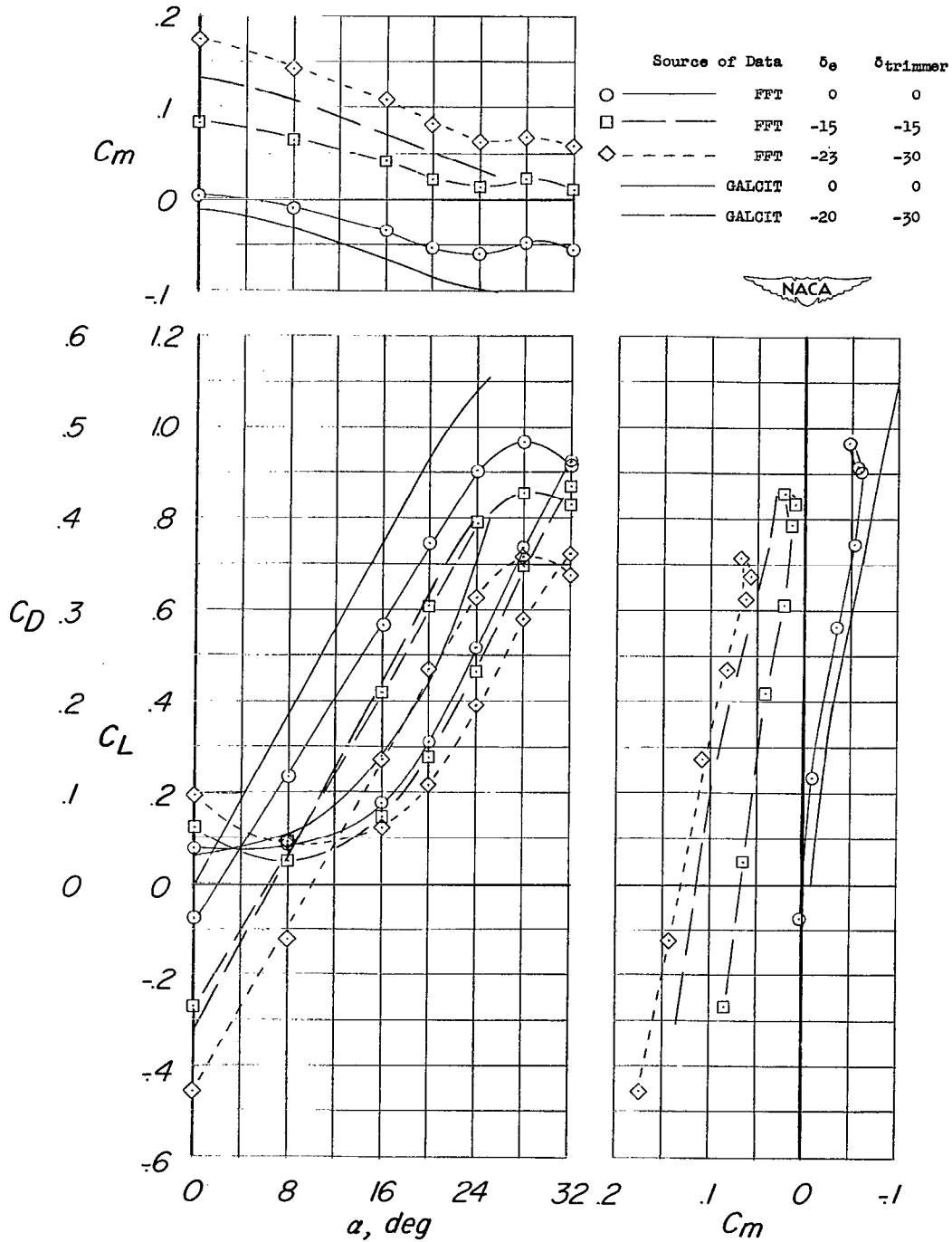


Figure 7.- Effect of elevon and trimmer deflection on the aerodynamic characteristics of a $\frac{1}{10}$ -scale model of the XF4D-1 airplane tested in the Langley free-flight tunnel and a 0.1791-scale model tested at GALCIT. Slats extended.

		Source of Data	δ_e	$\delta_{trimmer}$	Tail	
○	-----	FFT	0	0	on	
□	-----	FFT	-15	-30	on	
◇	-----	FFT	-15	-30	on+extension	
△	-----	FFT	-15	-30	off	
			α	δ_e	$\delta_{trimmer}$	Tail
		-----	0	0	0	on
		-----	10	-8	0	
		-----	15	-18	0	
		-----	20	-25	0	
		-----	-do-	-do-	-do-	off

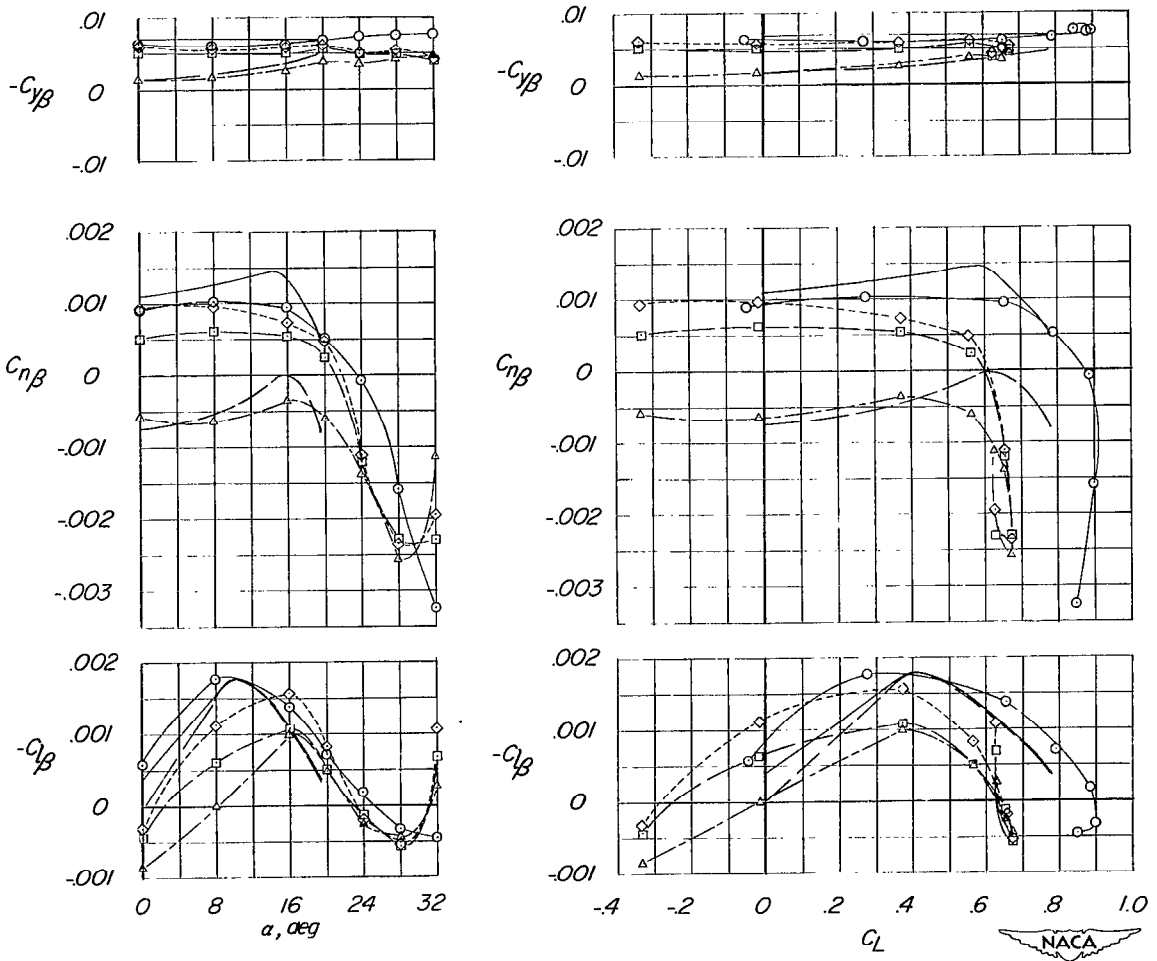


Figure 8.- Effect of angle of attack and lift coefficient on the lateral stability parameters of a $\frac{1}{10}$ -scale model of the XF4D-1 airplane tested in the Langley free-flight tunnel and a 0.1791-scale model tested at GALCIT. Slats retracted.

Source of Data		δ_e	$\delta_{trimmer}$	Tail
○	----- FFT	0	0	on
□	----- FFT	-23	-30	on
△	----- FFT	-23	-30	off

		a	δ_e	$\delta_{trimmer}$	Tail
-----	GALCIT	0	0	0	on
-----	GALCIT	10	-8	0	
-----	GALCIT	15	-18	0	
-----	GALCIT	20	-25	0	off
-----	GALCIT	-do-	-do-	-do-	off

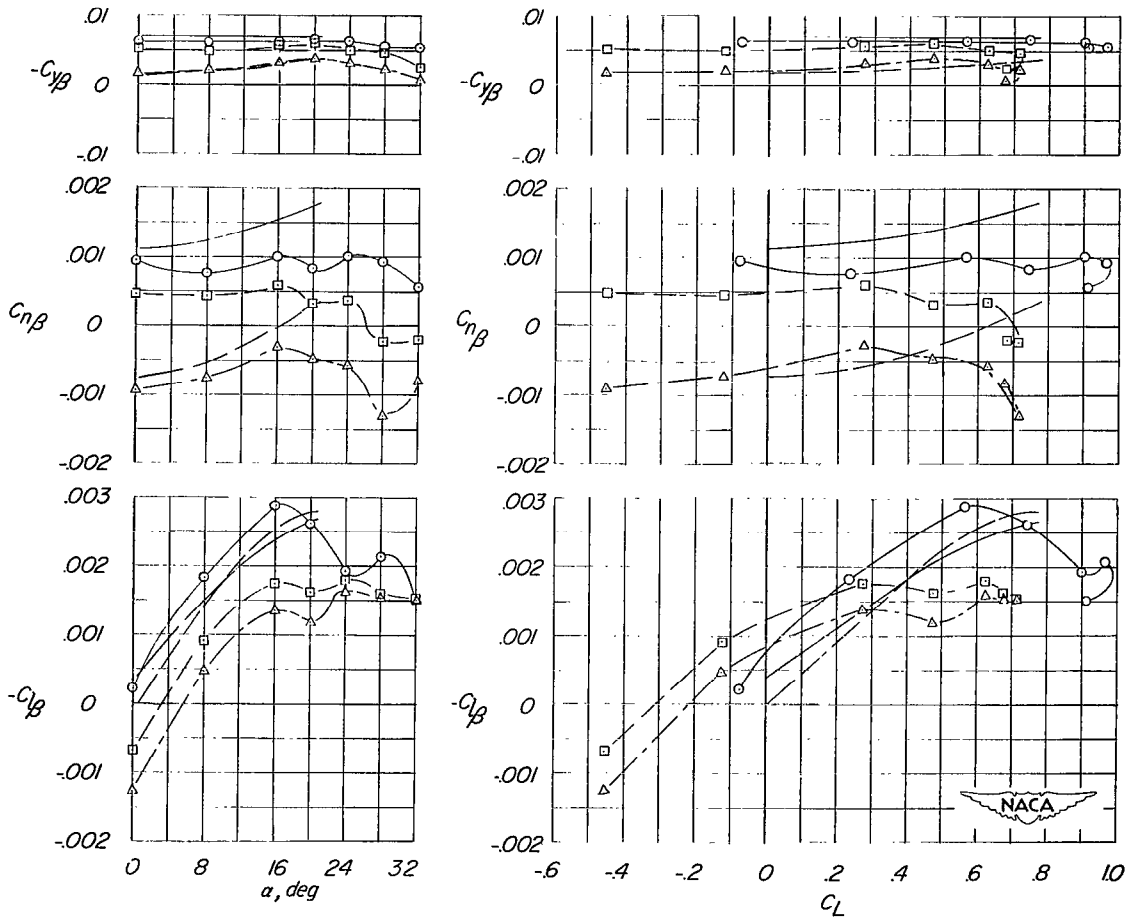


Figure 9.- Effect of angle of attack and lift coefficient on the lateral-stability parameters for a $\frac{1}{10}$ -scale model of the XF4D-1 airplane tested in the Langley free-flight tunnel and a 0.1791-scale model tested at GALCIT. Slats extended.

	Source of Data	δ_e , deg	δ_a , deg	$\delta_{trimmer}$, deg	Slats
○	FFT	-15	± 15	-30	Retracted
□	FFT	-23	± 15	-30	Extended
—	GALCIT	-15	± 15	0	Retracted
—	GALCIT	-23	± 15	0	Extended

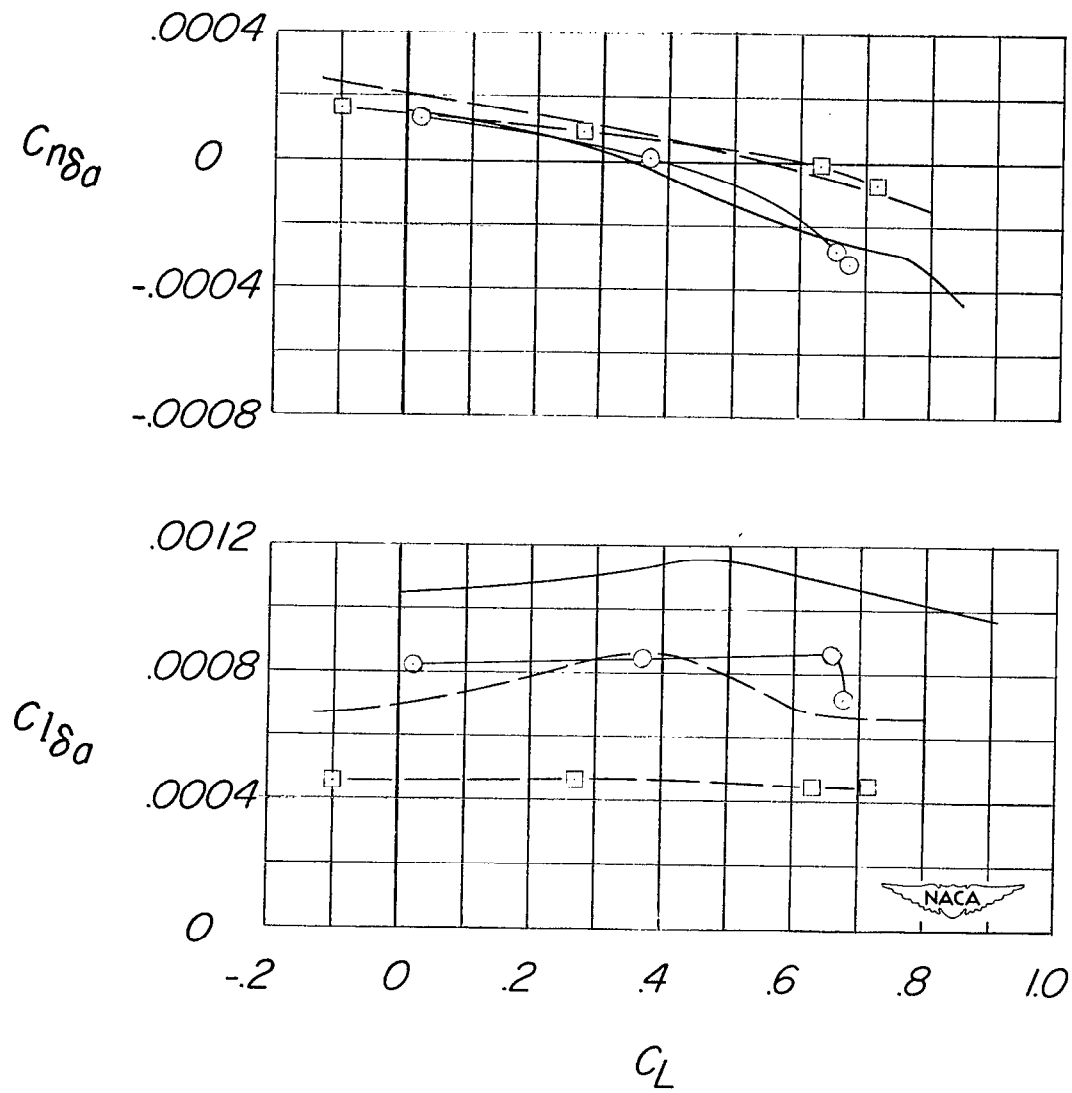
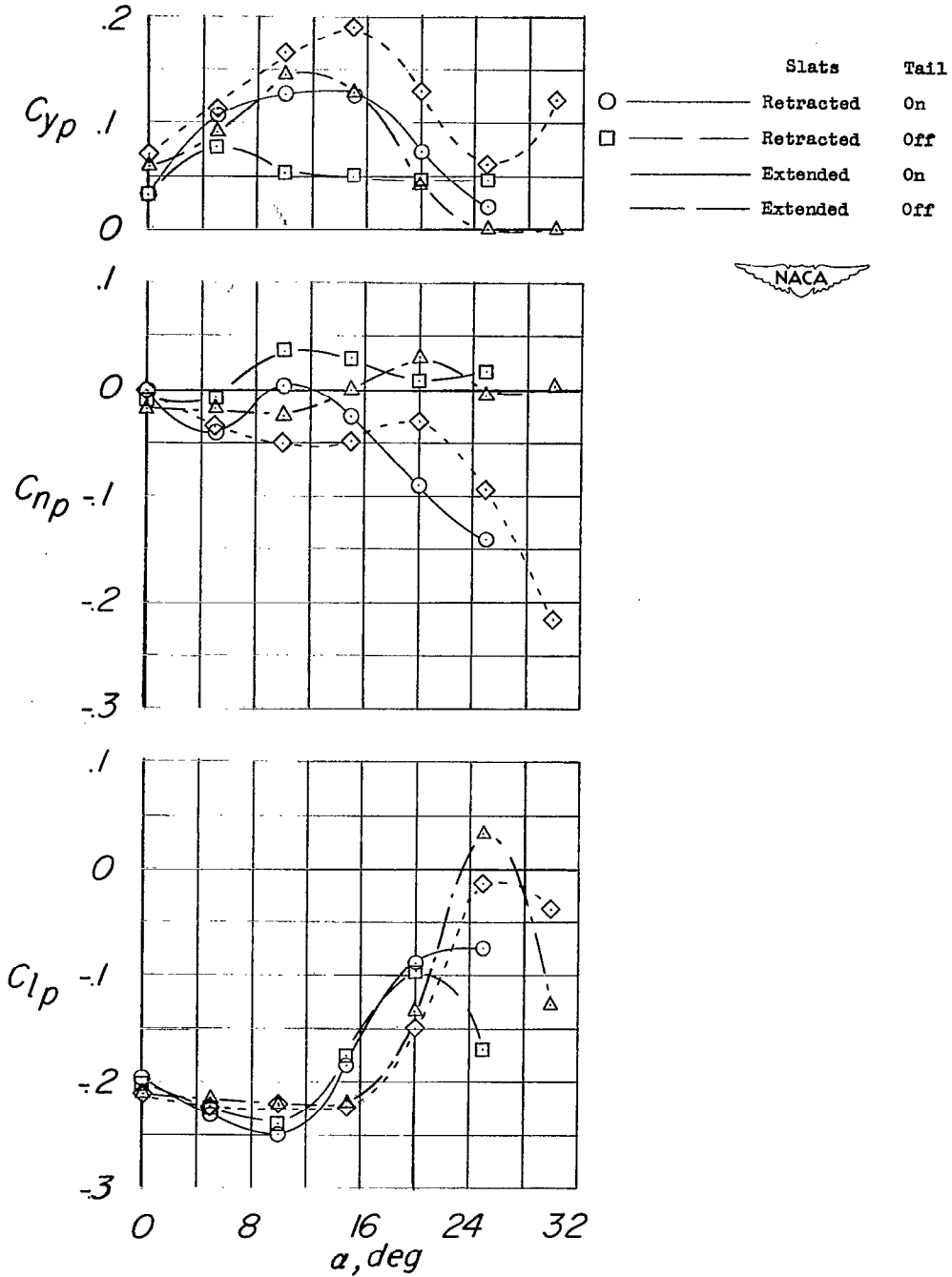
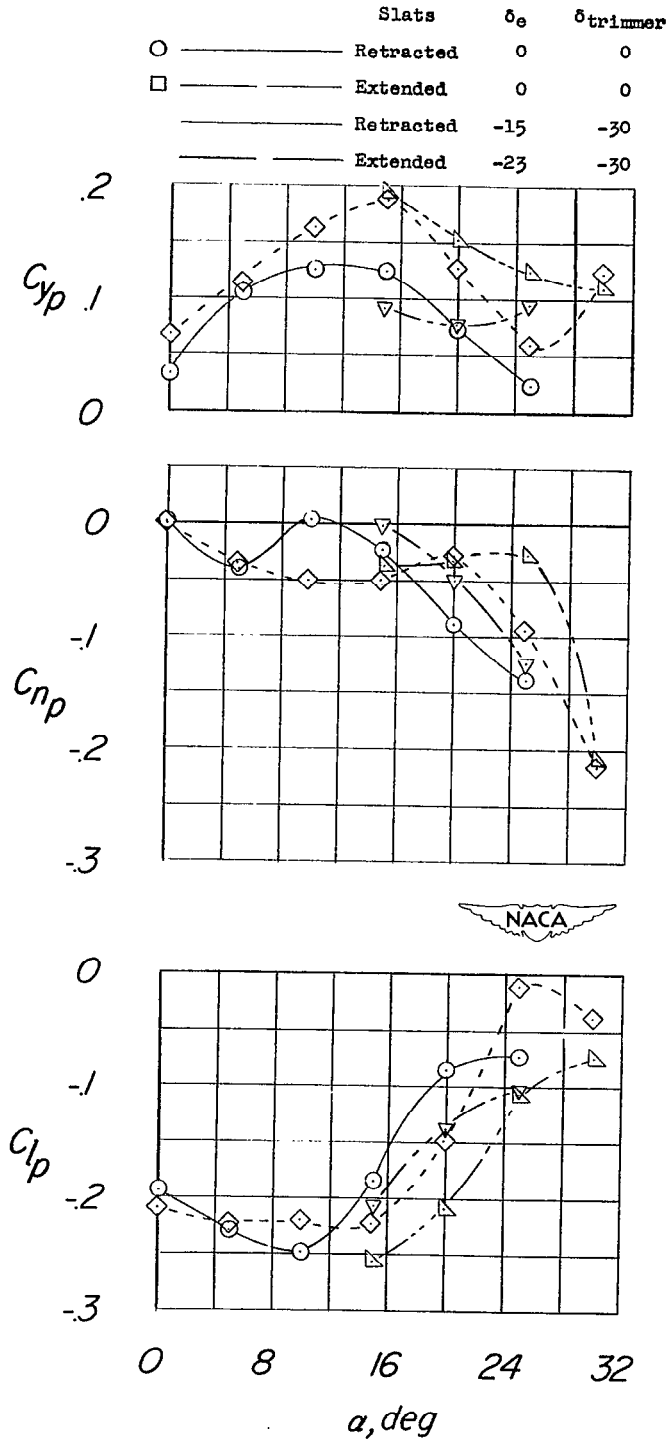


Figure 10.- Variation of the aileron effectiveness with lift coefficient for a $\frac{1}{10}$ -scale model of the XF4D-1 airplane tested in the free-flight tunnel and a 0.1791-scale model tested at GALCIT.



(a) Effect of vertical tail. $\delta_e = 0$; $\delta_{trimmer} = 0$.

Figure 11.- Variation of the rotary derivatives with angle of attack for a $\frac{1}{10}$ -scale model of the XF4D-1 airplane tested in the Langley free-flight tunnel.



(b) Effect of control deflections; vertical tail on.

Figure 11.- Concluded.

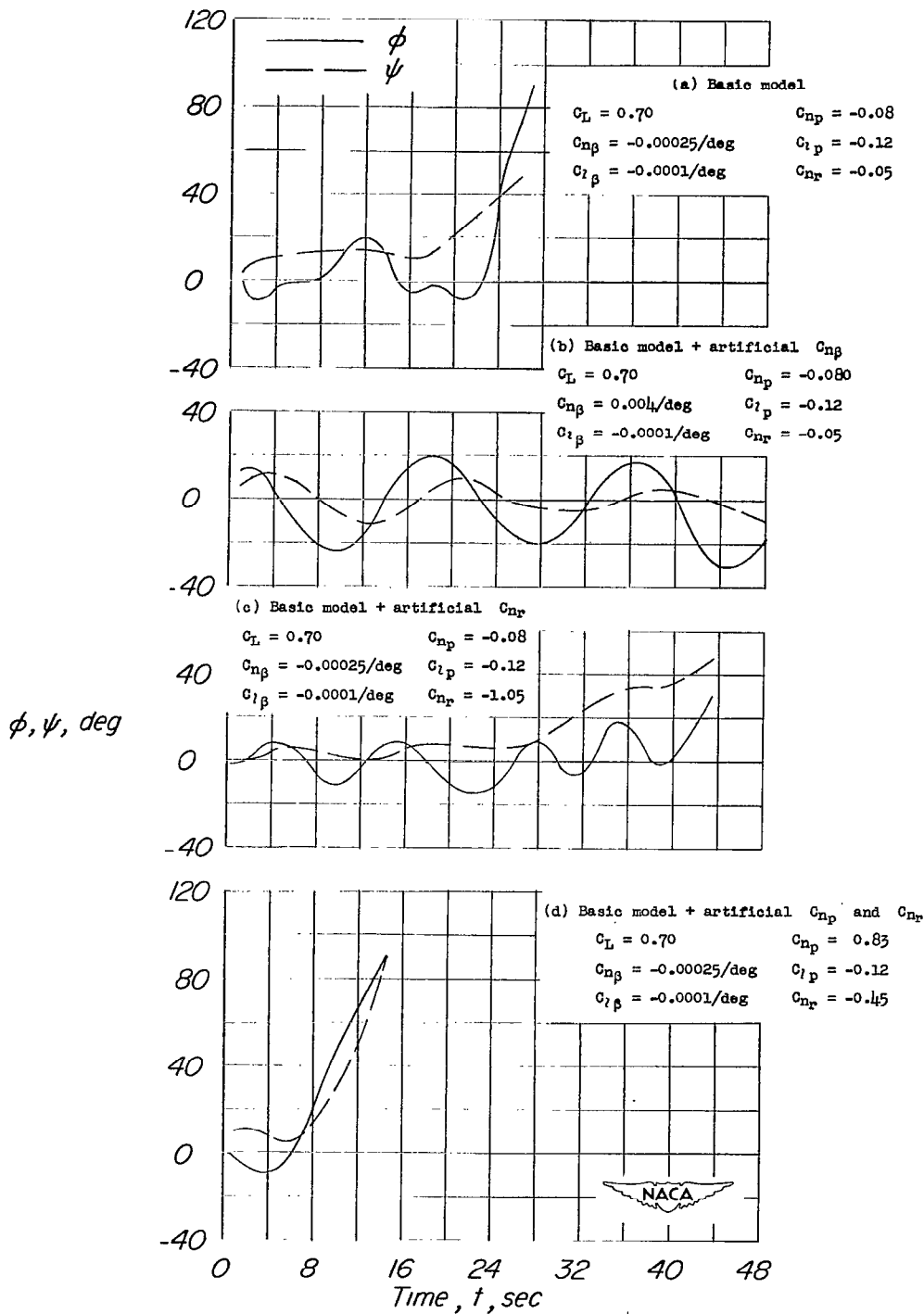


Figure 12.- Effect of several artificial stabilizing devices on the flight behavior of the $\frac{1}{10}$ -scale model of the XF4D-1 airplane tested in the Langley free-flight tunnel. Slats retracted.

Source	Altitude	Slats
○	Sea level	Retracted
□	Sea level	Extended
◇	40,000 feet	Retracted
△	40,000 feet	Extended
▽	Sea level	Retracted
▷	40,000 feet	Retracted

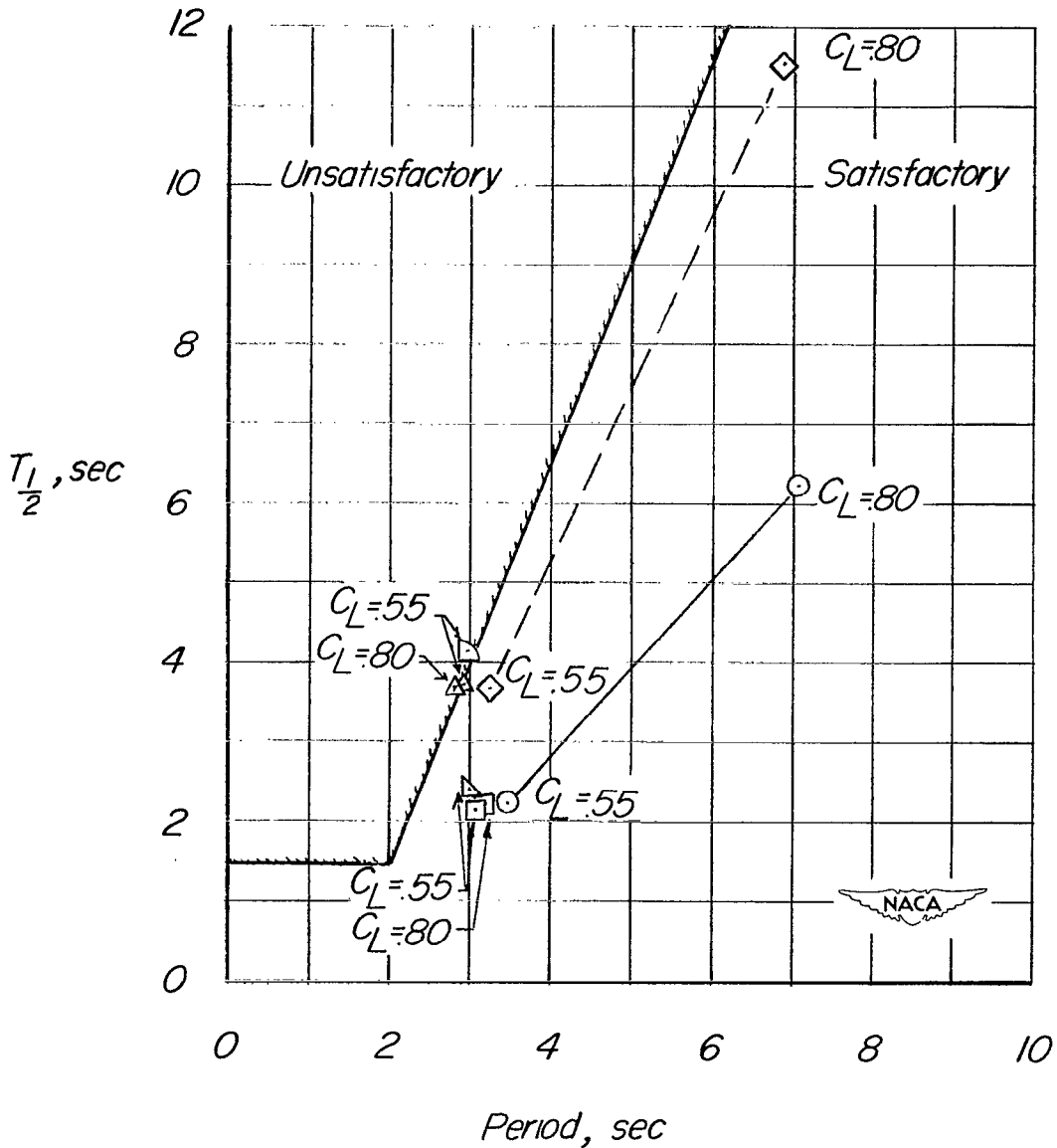


Figure 13.- Comparisons of the damping and period characteristics of the Douglas XF4D-1 airplane with the U. S. Navy flying-qualities specifications (reference 11).

SECURITY INFORMATION

NASA Technical Library



3 1176 01438 5604

~~CONFIDENTIAL~~